J Mater Sci (2015) 50:366–373
DOI 10.1007/s10853-014-8595-3

Influence of Al doping in $LaCoO_3$ on structural, electrical and magnetic properties

Aswin V. · Pramod Kumar · Pooja Singh · Anurag Gupta · S. Rayaprol · Anjana Dogra

Received: 20 June 2014 / Accepted: 8 September 2014 / Published online: 17 September 2014

Abstract We report investigations on polycrystalline $LaCo_{1-x}Al_xO_3$ ($x = 0$–0.9) bulk samples. The solid state synthesized samples showed a coexistence of rhombohedral and monoclinic phases in the intermediate concentrations ($0.2 \leq x \leq 0.5$) and pure rhombohedral phase otherwise. The observed effect of Al doping on *dc* transport has been analysed on the basis of small polaron hopping mechanism. The magnetisation results presented give evidence of weak ferromagnetism and anomalous temperature dependence of coercivity which we associate to the canting of the localised high-spin Co(III) and anti-symmetric exchange interactions at low temperatures.

Introduction

Lanthanum Cobaltate ($LaCoO_3$) has been an intriguing subject of research primarily because of the spin state equilibria and the anomalous magnetic behaviour accompanying this crossover [1–11]. The oxygen octahedra coordinating the cobalt ion in the prototypical perovskite structure controls the delicate balance between the Hund's coupling and the crystal field splitting energy for the *d* electrons of Co^{3+} [12]. At low temperatures (below $\sim$100 K), the latter dominates with Co^{3+} remaining in its low spin state (LS) ($t_{2g}^6 e_g^0$), where the compound is a diamagnetic semiconductor. With gradual rise in temperature, *d* electrons overcome the crystal field splitting, and Co^{3+} can either evolve into an intermediate ($t_{2g}^5 e_g^1$) (IS) or a high ($t_{2g}^4 e_g^2$) (HS) spin state. The excited states attain dominance at a temperature of $\sim$100 K (first spin state transition) manifested by a maximum in the magnetic susceptibility data and a Curie–Weiss-like temperature dependence afterwards [13]. The susceptibility data show another hump at $\sim$500 K followed by an increase in the effective magnetic moment [4]. This can be seen as the second spin state transition which is also the onset of an insulator to metallic transition [6]. These observations were explained initially by considering a LS–HS spin state transition at $\sim$100 K where there exists a dynamic ordering of HS and LS Co^{3+} in the temperature interval of 110–350 K and a quasistatic ordering of HS and IS Co^{3+} in the metallic phase >650 K [4]. Since Korotin et al. demonstrated the stability of an orbitally ordered IS state over HS state through LDA + U calculations [14], the researchers divided themselves into two sides of the balance. In this scenario, the first excitation at $\sim$100 K occurs to an orbitally ordered IS state. The debate is still evenly matched where we cannot rule out either of these conclusively even after thorough studies on almost all physical properties in and around the spin state transition [4, 5, 7, 10, 15–19].

Besides $LaCoO_3$, numerous studies have been carried out on divalent substitution in $La_{1-x}A_xCoO_3$, where *A* refers to divalent Sr, Ca or Ba. Such charge carrier doping modifies the magnetic ground state as well as renders the system metallic above a particular value of doping concentration (x) [20–24]. But with *B* site doping of the ABO_3 structure, there has not been such a comprehensive discussion regarding the structural as well as transport

Aswin V. · P. Kumar · P. Singh · A. Gupta · A. Dogra (✉)
National Physical Laboratory (CSIR), Dr. K. S. Krishnan Marg, New Delhi 110 012, India
e-mail: anjanad@nplindia.org

S. Rayaprol
UGC-DAE CSR, Mumbai Center, R-5 Shed, BARC, Trombay, Mumbai 400085, India

properties. The magnetic properties of lightly doped $LaCo_{1-x}M_xO_3$ ($x \leq 0.1$) (M = Al, Cr, Ga, Fe, Mn, Ni) were studied by Madhusudan et al. [25] and Vasanthacharya et al. [26] where they found that the temperature independent activation energy for the spin state transition increased considerably with the addition of Al and Cr while stabilizing the LS states Co^{3+}. Later, Kyomen et al. [27] in the light of the results of Al and Ga substitution in $LaSrCoO_4$ by Demazeau et al. [28] comprehended this stabilization as arising from the weaker covalency of Al–O bond and Ga–O bonds compared to Co–O bonds. A similar substitution of Rh on the other hand stabilizes the HS states of Co(III) [27, 29]. Motivated by these results we have performed a systematic investigation of polycrystalline $LaCo_{1-x}Al_xO_3$ (x = 0, 0.2, 0.3, 0.5, 0.8, 0.9) with special emphasis to the structural, morphological and *dc* transport mechanism. In light of these results further, we have re-examined the magnetic susceptibility data.

Materials and methods

Investigations were carried out on polycrystalline bulk samples of $LaCo_{1-x}Al_xO_3$ (x = 0, 0.2, 0.3, 0.5, 0.8, 0.9) synthesized by conventional solid state reaction of starting compounds. The La_2O_3, Al_2O_3 and Co_3O_4 (Alfa-Aesar) compounds with purity better than 99.99 % were used without further processing. Starting compounds taken in stoichiometric proportions were mixed and grinded thoroughly using an agate mortar pestle and pre-sintered at 800 °C for 12 h. The resultant powder was sintered at 1200 °C for 12 h after thorough grinding. All sintering steps were carried out in air with a ramp rate of 5 °C/min. The final sintering of the samples was carried out in pellet form (compressed into cylindrical pellets by uni-axial compaction at 12 tons) at 1300 °C for 12 h.

Structural studies on the resultant material were performed by powder X-ray diffraction (PXRD) using Rigaku MiniFlex-II tabletop diffractometer employing Cu–K_α radiation. PXRD data were analysed using Rietveld refinement method using the FullProf software [30]. The topographs of the samples were taken using ZEiss Evo MA10 scanning electron microscopy (SEM) with Oxford energy dispersive X-ray (EDAX) attachment which was also used to determine the elemental composition of the samples. The low temperature *dc* transport measurements were done on the pellets with a closed cycle refrigerator of APD cryogenics from room temperature down to 100 K using a Keithley 220 programmable current source and 2182A nano-voltmeter in four probe configuration with a Scientific instruments 9700 temperature controller. The measurements were performed by giving a constant current of 1 or 0.1 μA in the absence of magnetic field. Pellets of size approximately 4 × 7 mm were used in case of bulk samples, and linear contacts were made using silverpaste. The resistances of the samples were too high to measure using the present experimental setup below 100 K. The magnetic properties of the samples were investigated by a magnetic property measurement system (Quantum design-MPMS) magnetometer. The data were collected from 300 to 10 K at both a high field of 10 kOe and low field of 100 Oe.

Results and discussion

Powder X-ray diffraction

The structural properties for solid solution of $LaCo_{1-x}Al_xO_3$ were studied by analysing the PXRD data by Rietveld refinement method. The Rietveld refined PXRD profiles for the samples are shown in Fig. 1. Although most of the structure analysis of $LaCoO_3$ is based on a rhombohedral space group *R-3c* [31], there are reports which favour a monoclinic *I2/a* structure as well [32, 33]. The rhombohedral space group *R-3c* fits the $x = 0.0$ sample perfectly in our refinements. However, with the Al doping, a second monoclinic phase of *I2/a* space group also emerges for the intermediate concentrations ($0.2 \leq x \leq 0.5$). The profiles do not show any extra reflections other than those attributable to these two phases. The formation of inhomogeneous mixed phase samples for the intermediate concentrations can be indicative of the high distortion inherently induced in the system with the addition of Al. The phase fraction of rhombohedral and monoclinic phases change with changing dopant concentration (x) (Table 1).

The lattice parameters of the rhombohedral and monoclinic phases obtained from the refinement are presented in Tables 2 and 3, respectively. The PXRD profile shifts consistently towards right with increase in Al content due to the decreased ionic radii of Al^{3+} compared to Co^{3+}. This shift is visible in Fig. 2 where the highest intensity reflection centred $\sim 33°$ is shown. The doublet structure associated with undoped compound is also progressively reducing with increase in Al doping.

Composition and morphology

The SEM micrographs for samples with x = 0, 0.3, 0.5 and 0.8 are shown in Fig. 3. The information provided by these four micrographs is sufficient to conclude about the grain morphology of the complete set of samples. We observe that the grain morphology of the doped samples is random agglomerates joined together with the size of the agglomeration decreasing with Al concentration but in the pure

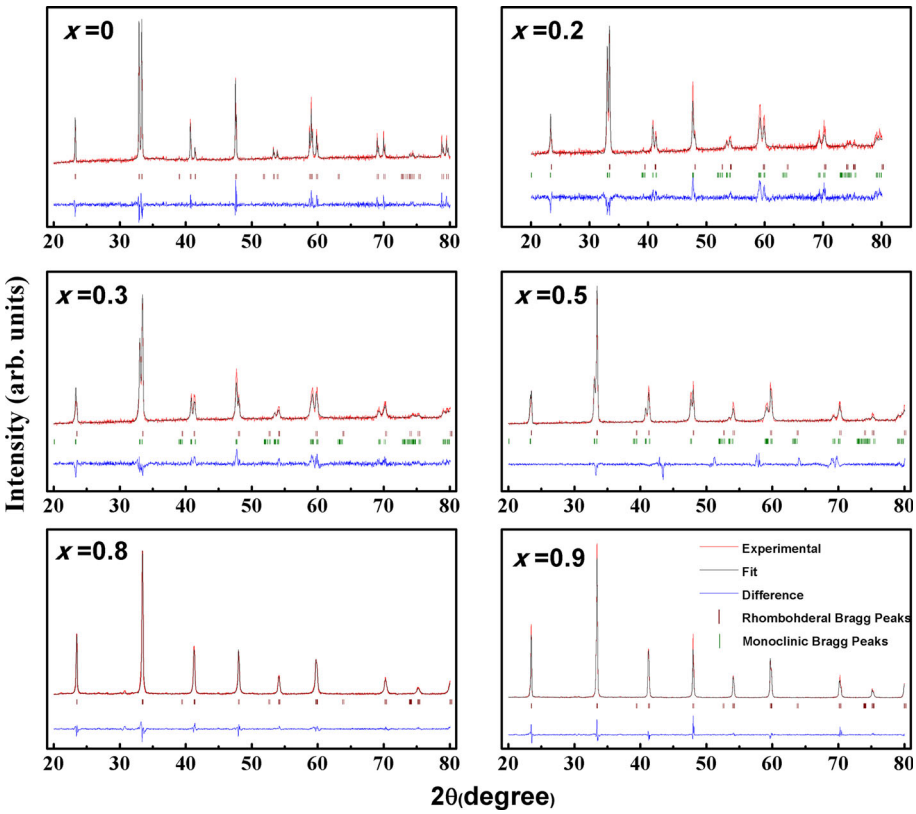

Fig. 1 Rietveld refined profiles for $LaAl_{1-x}Co_xO_3$ ($x = 0$–0.9). *Red lines* indicate the experimental data, *black curve* is the fitted data, *olive green lines* represent Bragg peaks and *blue line* is the difference between experimental and calculated data (Colour figure online)

Table 1 Fractional amount of Phases of $LaCo_{1-x}Al_xO_3$. The rhombohedral and monoclinic phases were of the space group *R-3c* (No.167) and *I2/a* (No.15), respectively

x	Fractional composition		χ^2
	Rhombohedral (R-3c)	*Monoclinic (I 2/a)*	
0	100	–	3.77
0.2	19.49	80.51	3.84
0.3	31.07	68.93	4.36
0.5	58.46	41.54	4.15
0.8	100	–	4.74
0.9	100	–	5.30

Table 2 Lattice parameters obtained from Rietveld refinement for the rhombohedral phase [*R-3c* (No.167)] of $LaCo_{1-x}Al_xO_3$

x	a (Å)	b (Å)	c (Å)
0	5.438 (6)	5.438 (6)	13.081 (5)
0.2	5.351 (7)	5.351 (7)	13.128 (6)
0.3	5.355 (5)	5.355 (5)	13.117 (5)
0.5	5.358 (8)	5.358 (8)	13.124 (5)
0.8	5.360 (1)	5.360 (1)	13.103 (8)
0.9	5.363 (3)	5.363 (3)	13.112 (2)

Table 3 Lattice parameters obtained from Rietveld refinement for monoclinic phase [*I2/a* (No.15)] of $LaCo_{1-x}Al_xO_3$

x	a (Å)	b (Å)	c (Å)	β (°)
0.2	5.364 (5)	5.425 (0)	7.625 (0)	90.82 (1)
0.3	5.367 (5)	5.417 (5)	7.637 (4)	90.88 (1)
0.5	5.371 (5)	5.419 (2)	7.637 (4)	90.87 (9)

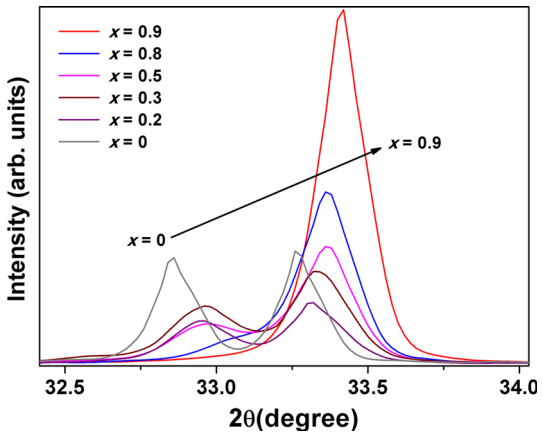

Fig. 2 The highest intensity peak of P-XRD for $LaCo_{1-x}Al_xO_3$ samples (Colour figure online)

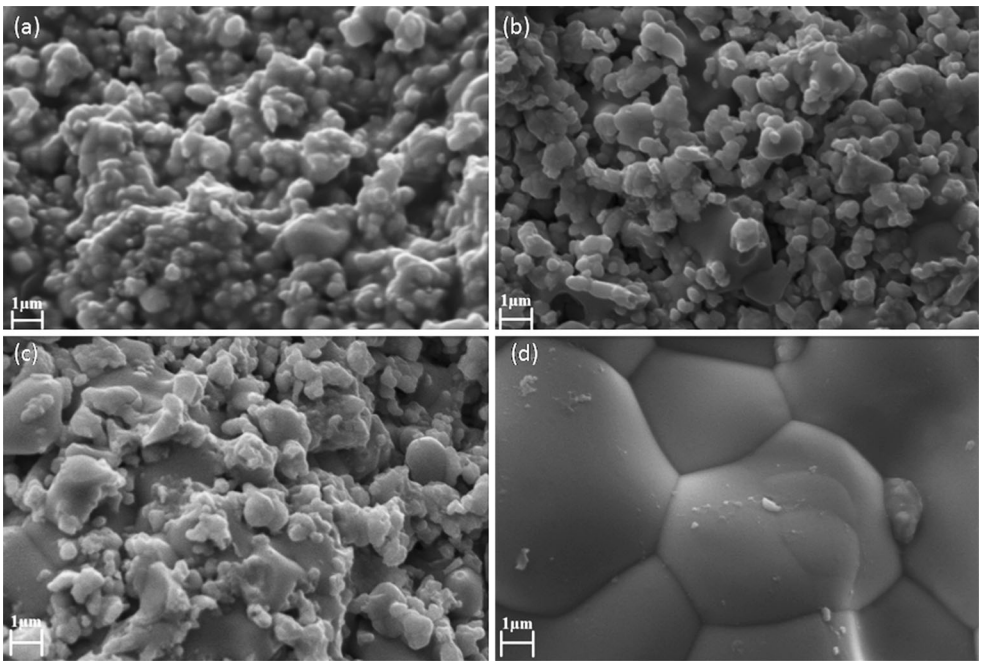

Fig. 3 SEM micrographs of $LaCo_{1-x}Al_xO_3$ **a** $x = 0.8$ **b** $x = 0.5$ **c** $x = 0.3$ **d** $x = 0$ at a magnification of 20 KX (Colour figure online)

Table 4 Tabulation of weight percentages obtained from EDAX and intended weight percentages for $LaCo_{1-x}Al_xO_3$ ($x = 0$, 0.3, 0.5, 0.8) calculated from the chemical formula

x	Weight % from EDAX			Weight % calculated		
	La	Al	Co	La	Al	Co
0	56.6 (6)	0	22.4 (6)	56.5	0	23.97
0.3	59.8 (2)	3.0 (5)	16.2 (5)	58.79	3.42	17.46
0.5	62.6 (7)	4.9 (5)	11.6 (7)	60.43	5.869	12.81
0.8	63.6 (1)	8.2 (4)	5.0 (8)	63.05	9.79	5.35

$LaCoO_3$ distinct shapes can be identified. The particle sizes are also found to decrease with increased Al doping. These morphological features also have an influence on the electrical and magnetic properties of the samples as we see in the subsequent discussions. The weight percentages obtained from EDAX are found to complement the actual doping weight percentages as shown in Table 4.

dc transport

The resistivity versus temperature profile of $LaCo_{1-x}Al_xO_3$ ($x = 0$–0.5) is presented in Fig. 4. The samples with high Al concentration ($x = 0.8$, 0.9) were excessively resistive to be measured by the current experimental setup. These insulating samples do not feature in the following discussion. The resistivity behaviour of pure $LaCoO_3$ complements well with the previous experimental work where it gradually increases with decreasing temperature like a semiconductor. The conduction in LaCoO3 has been

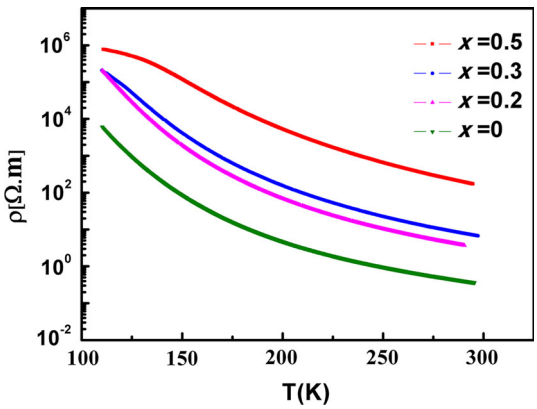

Fig. 4 Resistivity temperature profile of $LaCo_{1-x}Al_xO_3$ (Colour figure online)

attributed to small polaron hopping mechanism as suggested by the previous works where small polarons of holes are generated by the electron excitation from the narrow π* bands of Low Spin Co (III) to the σ* band of the e_g orbital of the Co 3d excited states [4, 34].

Partial substitution of Al for Co results in increase in the resistivity of the samples. With increasing Al content, resistivity is gradually increasing. A straight forward reason for this increase is the progressive reduction of carriers [which as we know are small polarons of holes in π* bands of Low Spin Co(III)] on account of Al substitution at Co sites. Along with this it is also worth mentioning that Al substitution stabilizes the low spin states by a negative cooperative effect [27] which reduces the occupancy of e_g orbitals and

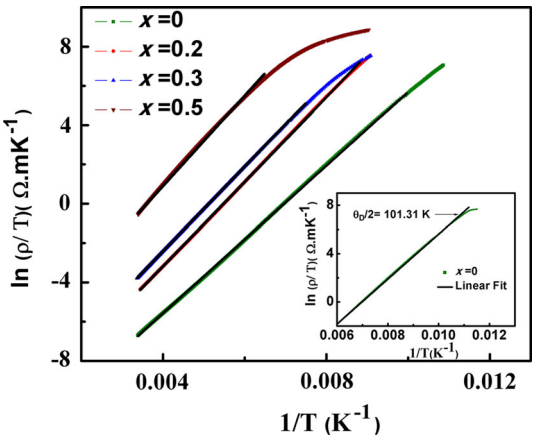

Fig. 5 Arrhenius Plot for small polaron hopping conduction for $LaCo_{1-x}Al_xO_3$ ($x = 0$–0.5). The calculation of Debye temperatures for $x = 0$ sample is shown in the inset (Colour figure online)

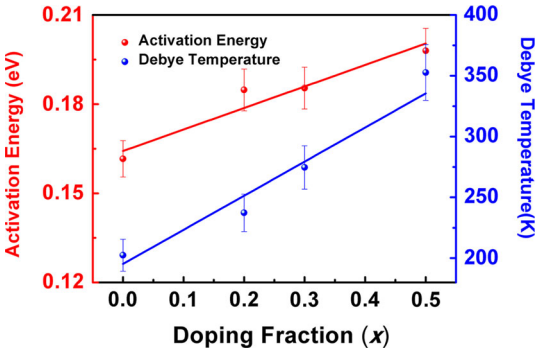

Fig. 6 Variation of Activation energies and Debye temperatures calculated from the small polaron fit with doping fraction (Colour figure online)

thus implicitly reducing the carrier concentration. However, the grain boundary contribution towards resistivity cannot be neglected as the SEM micrographs reveal that the particle size reduces with increasing Al concentrations which enhance grain boundary scattering and increase resistivity. To further corroborate the small polaron scenario, we have shown the Arrhenius plots (Fig. 5) for the small polaron hopping model fitted according to the equation [35, 36].

$$\rho = \rho_\alpha T e^{\frac{E_p}{k_B T}} \quad (1)$$

where ρ is the resistivity of the sample, $\rho_\alpha = \left(\frac{k_B}{\upsilon_{ph} N^2 e^2 R^2 C(1-C)}\right) e^{2\alpha R}$, k_B is the Boltzmann constant, E_p is the activation energy and T is the absolute temperature. N is the number of ion sites per unit volume, R is the average intersite spacing obtained from the relation $R = (1/N)^{1/3}$, C is the fraction of sites occupied by a polaron, α is the electron wave function decay constant obtained from fitting the experimental conductivity data, υ_{ph} is the optical phonon frequency. The activation energies

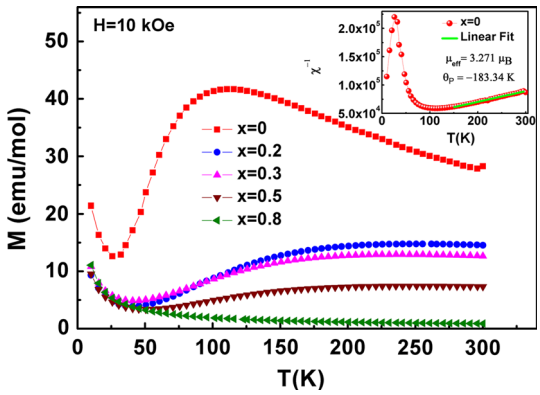

Fig. 7 M–T curves for $LaCo_{1-x}Al_xO_3$($x = 0$–0.8) (ZFC mode) at 10 kOe. The inset shows the inverse susceptibility curve for the sample $x = 0$ (Colour figure online)

required for hopping mechanism have been obtained from the slope of the straight line fit as shown in Fig. 5. We can also get the Debye temperature from the point in the Arrhenius plot where the curve loses linearity [35] (inset Fig. 5). The activation energy and Debye temperature obtained from the fitting are shown in Fig. 6. The table shows that the activation energies required for hopping conduction increase with increase in Al concentration. Similar increase in activation energies caused by doping has been reported in the literature [35–37] and has been explained on the basis of the localisation of the e_g electrons caused by doping.

Magnetisation

Figure 7 shows that the magnetisation data measured in an applied dc magnetic field of 10 kOe are plotted as a function of temperature. For the $x = 0.0$ sample, with decreasing temperature, there is gradual increase in magnetisation (M) from 300 to 110 K, and a sharp decrease below 110 K giving evidence of the spin state transition. M reaches the lowest value around 30 K, before increasing again as T is lowered further. No bifurcation was observed between zero field cooled (ZFC) and field cooled (FC) magnetisation curves of $LaCo_{1-x}Al_xO_3$ ($x = 0$–0.8) collected from 10 to 300 K, under this magnetic field strength. The effective moment of this parent compound determined from the Curie–Weiss fit of inverse susceptibility data for temperatures above 150 K is 3.27 μ_B per formula unit (see inset Fig. 7). These results are consistent with the earlier literature on $LaCoO_3$ [4, 38]. With Al doping concentration, this spin state transition is delayed and finally lost for a concentration of $x \geq 0.8$. The effect of Al doping in the spin state transition can be explained as follows, the increase in aluminium concentration reduces the magnetisation and suppresses the spin state transition by stabilising the low spin states of Co(III) hence increasing their

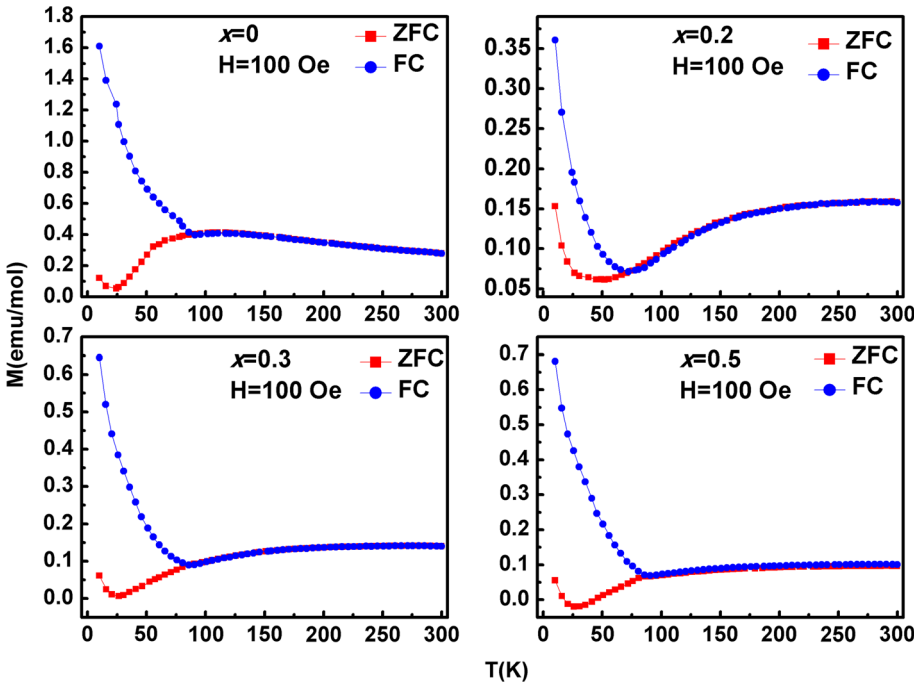

Fig. 8 The M–T curves of the samples $LaCo_{1-x}Al_xO_3$ ($x = 0$–0.5) at a field of 100 Oe exhibiting a bifurcation in the ZFC and FC data (Colour figure online)

number. This stabilization owes to the low covalency of the Al–O bond due to low electro negativity of aluminium compared to Cobalt [27]. Besides this the doping of Al is also found to increase the activation energy needed for the spin state transition as the smaller aluminium atoms increase the crystal field splitting energy [26, 27]. At higher Al concentrations ($\sim$0.8), any contribution of HS cobalt towards the moment is obscured by the paramagnetic signal of the dopant. Hence, the nature of magnetisation curves for samples having a doping concentration of x above 0.8 can be safely called paramagnetic.

The low field (100 Oe) magnetisation curves (Fig. 8) show features that are different in comparison to those at high fields. For all the samples with x up to $\sim$0.5, from the low field magnetisation curves, we find that the ZFC and FC data bifurcate at a temperature of $\sim$85 K, with FC data indicating a ferromagnetic ordering. The low temperature upturns in the M (T) at high fields mentioned above are still observed in the ZFC data taken in low fields (Fig. 8). Earlier in pure $LaCoO_3$, both the upturn behaviour and the ferromagnetism were attributed to the presence of localised HS spins stabilized either on an ideal reconstructed surface or on a water adsorbed surface [39, 40].The presence of the ferromagnetic order down to a doping fraction of $x = 0.5$ further confirms the role of localised Co spins on the ferromagnetic signal. Among the alternatives, we consider this localised spins to be of HS Co(III) which orders antiferromagnetically to give a weak canted spin-ferromagnetic moment. The following discussion on M–H loops substantiates this possibility.

The M–H loops, for all the samples with $x \leq 0.5$, measured at different temperatures are shown in Fig. 9. The observed hysteretic behaviour of the M–H loops at $T < 80$ K reaffirms the weak ferromagnetism up to a doping fraction of $x = 0.5$, consistent with the M–T data. The low temperature (10 and 25 K) M–H loops do not saturate even at a field of 10 kOe. At first glance, this appears to be due to the paramagnetic signal from the bulk. However, a thorough study associates this to the anti-ferromagnetic exchange interaction in the samples [38, 41], which also reinforces the above suggestion of antiferromagnetically ordered localised HS spins present in these systems. This is further supported by the fact that though the magnetic moment steadily increases with decreasing temperatures (<30 K), the coercivities show an inverse relationship with temperature for all these four samples. The coercivities extracted from the M–H loops are presented in Fig. 10. Such an anomalous behaviour of coercivity may arise due to an anti-symmetric exchange interaction which involves the LS Co(III) interacting with the excited HS Co(III) subsequently influencing the magneto-crystalline anisotropy and thereby reducing the coercive field [42]. To substantiate this, we derived the irreversible magnetisation from the FC and ZFC curves at 100 Oe. Irreversibility relates to the magnetic anisotropy present in the samples [43, 44]. The temperature dependence of relative irreversible magnetisation $(M_{FC}-M_{ZFC})/M_{FC}$ in Fig. 11 gives a maximum around $\sim$30 K for all samples after which it starts decreasing. Thus, the decrease after 30 K can be indicative of the reduction in the magnetic anisotropy which is the cause of the decrease in coercivity below these temperatures.

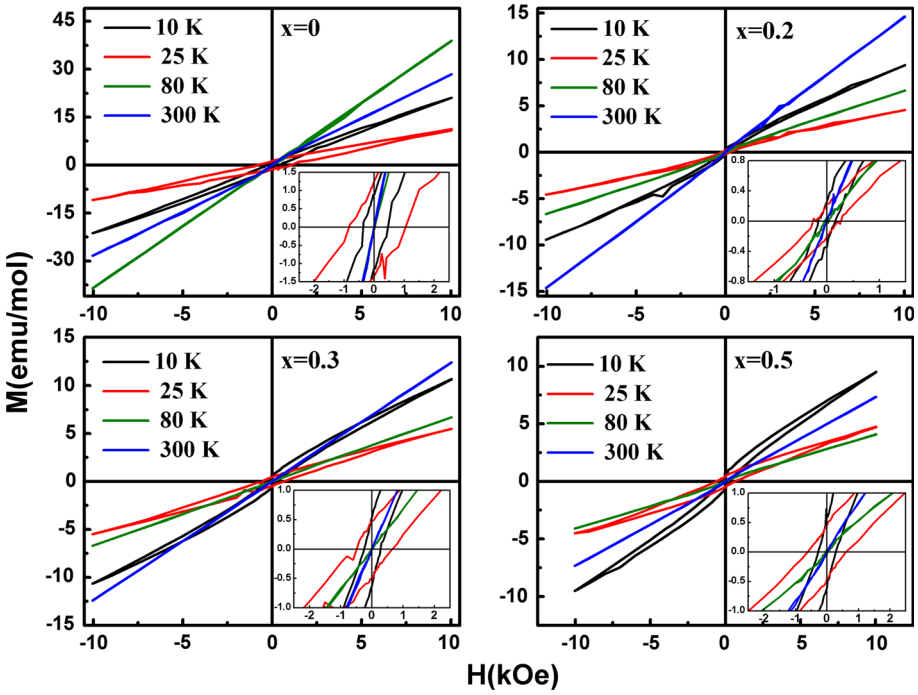

Fig. 9 M–H loops of $LaCo_{1-x}Al_xO_3(x = 0–0.5)$ at 10, 25, 80 and 300 K (Colour figure online)

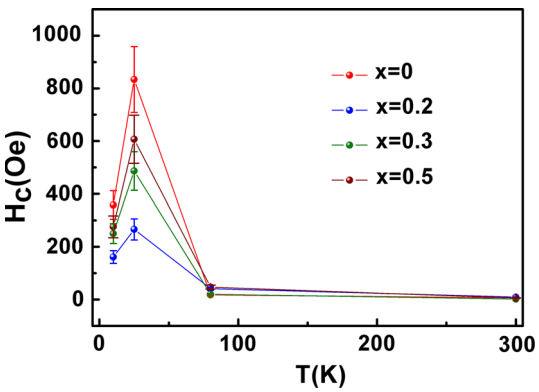

Fig. 10 Variation of coercive field (Hc) as a function of temperature for $LaCo_{1-x}Al_xO_3(x = 0–0.5)$ (Colour figure online)

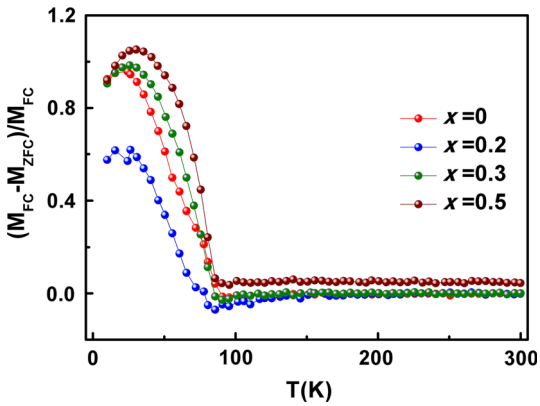

Fig. 11 Relative magnetic irreversibility as a function of temperature for $LaCo_{1-x}Al_xO_3(x = 0–0.5)$ (Colour figure online)

Conclusions

To conclude, we have synthesised samples of $LaCo_{1-x}Al_xO_3$ ($x = 0–0.9$) by solid state reaction synthesis. The structural analysis reveals phase coexistence of rhombohedral and monoclinic phases in the intermediate concentrations of $0.2 \leq x \leq 0.5$ and pure rhombohedral phase otherwise. The resistivity increases with Al doping owing to the increased activation energies required for small polaron hopping. The M–T curves and the M–H loops are in harmony where there exists a weak ferromagnetism up to a doping fraction of $x = 0.5$ at temperatures below $\sim$85 K. The observation of anomalous temperature dependence of coercivity below T < 30 K relates this weak ferromagnetism to the anti-ferromagnetic ordering of HS Co(III) surface spins, which undergoes anti-symmetric exchange interactions thereby reducing the magnetocrystalline anisotropy and hence the coercivity.

Acknowledgements The authors thank Prof. R.C. Budhani, DNPL for his encouragement and support. The authors greatly acknowledge Mr. Naval, Mr. Jai Tawale for the P-XRD and SEM micrographs, respectively. Aswin acknowledges CSIR for the financial support. AD acknowledges IFCPAR (4704-1) for the funding.

References

1. Goodenough JB (1958) An interpretation of the magnetic properties of the perovskite-type mixed crystals $La_{1-x}Sr_xCoO_{3-\lambda}$. J Phys Chem Solids 6:287–297

2. Raccah PM, Goodenough JB (1967) First-Order Localized-Electron ⇆ Collective-Electron Transition in $LaCoO_3$. Phys Rev 155:932–943
3. Abbate M, Fuggle JC, Fujimori A, Tjeng LH, Chen CT, Potze R, Sawatzky GA, Eisaki H, Uchida S (1993) Electronic structure and spin-state transition of $LaCoO_3$. Phys Rev B 47:16124–16130
4. Señarís-Rodríguez MA, Goodenough JB (1995) $LaCoO_3$ Revisited. J Solid State Chem 116:224–231
5. Stølen S, Grønvold F, Brinks H, Atake T, Mori H (1997) Energetics of the spin transition in $LaCoO_3$. Phys Rev B 55:14103–14106
6. Tokura Y, Okimoto Y, Yamaguchi S, Taniguchi H, Kimura T, Takagi H (1998) Thermally induced insulator-metal transition in LaCoO3: a view based on the Mott transition. Phys Rev B 58:R1699–R1702
7. Haverkort MW, Hu Z, Cezar JC, Burnus T, Hartmann H, Reuther M, Zobel C, Lorenz T, Tanaka A, Brookes NB, Hsieh HH, Lin HJ, Chen CT, Tjeng LH (2006) Spin state transition in $LaCoO_3$ studied using soft X-ray absorption spectroscopy and magnetic circular dichroism. Phys Rev Lett 97:176405
8. Podlesnyak A, Streule S, Mesot J, Medarde M, Pomjakushina E, Conder K, Tanaka A, Haverkort MW, Khomskii DI (2006) Spin-state transition in $LaCoO_3$: direct neutron spectroscopic evidence of excited magnetic states. Phys Rev Lett 97:247208
9. Kozlenko DP, Golosova NO, Jirák Z, Dubrovinsky LS, Savenko BN, Tucker MG, Le Godec Y, Glazkov VP (2007) Temperature- and pressure-driven spin-state transitions in $LaCoO_3$. Phys Rev B 75:064422
10. Tachibana M, Yoshida T, Kawaji H, Atake T, Takayama-Muromachi E (2008) Evolution of electronic states in $RCoO_3$ (R = rare earth): heat capacity measurements. Phys Rev B 77:094402
11. Liu ST, Wu Y, Jia YQ (1993) Spin and valence state equilibria of cobalt and magnetic properties of $LaCoO_3$. J Alloys Compd 200:71–176
12. Bhide VG, Rajoria DS, Rao GR, Rao CNR (1972) Mössbauer studies of the high-spin-low-spin equilibria and the localized-collective electron transition in $LaCoO_3$. Phys Rev B 6:1021–1032
13. Asai K, Gehring P, Chou H, Shirane G (1989) Temperature-induced magnetism in $LaCoO_3$. Phys Rev B 40:10982–10985
14. Korotin MA, Ezhov SY, Solovyev IV, Anisimov VI, Khomskii DI, Sawatzky GA (1996) Intermediate-spin state and properties of $LaCoO_3$. Phys Rev B 54:5309–5316
15. Zobel C, Kriener M, Bruns D, Baier J, Gruninger M, Lorenz T, Reutler P, Revcolevschi A (2002) Evidence for a low-spin to intermediate-spin state transition in $LaCoO_3$. Phys Rev B 66:020402
16. Radaelli PG, Cheong SW (2002) Structural phenomena associated with the spin- state transition in $LaCoO_3$. Phys Rev B 66:094408
17. Asai K, Yokokura O, Nishimori N, Chou H, Tranquada JM, Shirane G, Higuchi S, Okajima Y, Kohn K (1994) Neutron-scattering study of the spin-state transition and magnetic correlations in $La_{1-x}Sr_xCoO_3$ ($x = 0$ and 0.08). Phys Rev B 50:3025–3032
18. Knížek K, Novák P, Jirák Z (2005) Spin state of $LaCoO_3$: dependence on CoO_6 octahedra geometry. Phys Rev B 71:054420
19. Ishikawa A, Nohara J, Sugai S (2004) Raman Study of the orbital-phonon coupling in $LaCoO_3$. Phys Rev Lett 93:136401
20. Kriener M, Zobel C, Reichl A, Baier J, Cwik M, Berggold K, Kierspel H, Zabara O, Freimuth A, Lorenz T (2004) Structure, magnetization, and resistivity of $La_{1-x}M_xCoO_3$ (M = Ca, Sr, and Ba). Phys Rev B 69:094417
21. Wu J, Leighton C (2003) Glassy ferromagnetism and magnetic phase separation in $La_{1-x}Sr_xCoO_3$. Phys Rev B 67:174408
22. Zeng R, Debnath JC, Chen DP, Shamba P, Wang JL, Kennedy SJ, Campbell SJ, Silver T, Dou SX (2011) Magnetic properties in polycrystalline and single crystal Ca-doped $LaCoO_3$. J Appl Phys 109:07E146
23. Baio G, Barucca G, Caciuffo R, Rinaldi D, Mira J, Rivas J, Señarís-Rodríguez MA, Fiorani D (2000) Phase separation, thermal history and magnetic behaviour of Sr doped $LaCoO_3$. J Phys 12:9761–9770
24. Phelan D, Louca D, Kamazawa K, Hundley MF, Yamada K (2007) Influence of the ionic size on the evolution of local Jahn-Teller distortions in cobaltites. Phys Rev B 76:104111
25. Madhusudan WH, Vasanthacharya NY, Ganguly P (1980) Spin-state equilibrium in lanthanum cobaltate-effect of magnetic and non-magnetic near-neighbour impurities. Indian J Chem 19A:1037–1041
26. Vasanthacharya NY, Ganguly P (1983) Near-Neighbour impurity effect on the spin state transitions in $LaCoO_3$ at low temperature ($12 < T < 300$ K). Bull Mater Sci 5:307–315
27. Kyomen T, Asaka Y, Itoh M (2003) Negative cooperative effect on the spin-state excitation in $LaCoO_3$. Phys Rev B 67:144424
28. Demazeau G, Pouchard M, Li-Ming Z, Hagenmuller P (1987) New Cobalt(III) Oxides: $A_{0.5}La_{1.5}Mg_{0.5}Co_{0.5}O_4$, ($A$ = Ca, Sr, Ba). Analysis and discussion of the Low Spin → High Spin Transition. Z Anorg Allg Chem 555:64–78
29. Knížek K, Hejtmánek J, Maryško M, Jirák Z, Buršík J (2012) Stabilization of the high-spin state of Co^{3+} in $LaCo_{1-x}Rh_xO_3$. Phys Rev B 85:134401
30. Rietveld HM (1969) A profile refinement method for nuclear and magnetic structures. J Appl Cryst 2:65–71
31. Vogt T, Hriljac JA, Hyatt NC, Woodward P (2003) Pressure-induced intermediate-to-low spin state transition in $LaCoO_3$. Phys Rev B 67:140401(R)
32. Maris G, Ren Y, Volotchaev V, Zobel C, Lorenz T, Palstra TTM (2003) Evidence for orbital ordering in $LaCoO_3$. Phys Rev B 67:224423
33. Wang Y, Fan HJ (2010) Orbital ordering-driven ferromagnetism in $LaCoO_3$ nanowires. J Appl Phys 108:053917
34. Iguchi E, Ueda K, Jung WH (1996) Conduction in $LaCoO_3$ by small-polaron hopping below room temperature. Phys Rev B 54:17431–17437
35. Banerjee A, Pal S, Chaudhuri BK (2001) Nature of small-polaron hopping conduction and the effect of Cr doping on the transport properties of rare-earth manganite. J Chem Phys 115:1550–1558
36. Khan W, Naqvi AH, Gupta M, Husain S, Kumar R (2011) Small polaron hopping conduction mechanism in Fe doped $LaMnO_3$. J Chem Phys 135:054501
37. Pi L, Zheng L, Zhang Y (2000) Transport mechanism in polycrystalline $La_{0.825}Sr_{0.175}Mn_{1-x}Cu_xO_3$. Phys Rev B 61:8917–8921
38. Schmidt R, Wu J, Leighton C, Terry I (2009) Dielectric response to the low-temperature magnetic defect structure and spin state transition in polycrystalline $LaCoO_3$. Phys Rev B 79:125105
39. Yan JQ, Zhou JS, Goodenough JB (2004) Ferromagnetism in $LaCoO_3$. Phys Rev B 70:014402
40. Harada A, Taniyama T, Takeuchi Y, Sato T, Kyômen T, Itoh M (2007) Ferromagnetism at the surface of a $LaCoO_3$ single crystal observed using scanning SQUID microscopy. Phys Rev B 75:184426
41. Tiwari B, Surendra MK, Rao MSR (2013) $HoCrO_3$ and $YCrO_3$: a comparative study. J Phys 25:216004
42. du Trémolet de Lacheisserie E, Gignoux D, Schlenker M (2005) Magnetism: Materials and Applications, XXIV. Springer, New York
43. Wang LC, Dong QY, Mo ZJ, Xu ZY, Hu FX, Sun JR, Shen BG (2013) Low-temperature reversible giant magnetocaloric effect in the HoCuAl compound. J Appl Phys 114:163915
44. Bora T, Ravi S (2014) Negative magnetization and the tunable exchange bias field in $LaCr_{0.8}Mn_{0.2}O_3$. J Magn Magn Mater 358–359:208–211